



Cite this: *RSC Adv.*, 2017, 7, 35845

# Improved osseointegrating functionality of cell sheets on anatase TiO<sub>2</sub> nanoparticle surfaces

Ying Wang,<sup>a</sup> Zhiwei Jiang,<sup>b</sup> Ke Yu,<sup>b</sup> Yuting Feng,<sup>b</sup> Yue Xi,<sup>b</sup> Kaichen Lai,<sup>b</sup> Tingben Huang,<sup>b</sup> Huiming Wang<sup>c</sup> and Guoli Yang<sup>b</sup>  <sup>\*</sup>

Bone marrow mesenchymal stem cell sheets (BMSC sheets) have been reported as a powerful tool for bioengineering applications in accelerating osseointegration. TiO<sub>2</sub> nanoparticles are beneficial for osteogenic differentiation of bone marrow mesenchymal stem cells (BMSCs) *in vitro*. Nonetheless, no studies have reported the effects of anatase TiO<sub>2</sub> nanoparticles on the osseointegrating functionality of BMSC sheets *in vitro* and *in vivo*. This study is designed to verify the osteogenesis enhancing effects of TiO<sub>2</sub> nanoparticle coated implants on BMSC sheets. In this study, we used a novel light-induced cell sheet method to fabricate BMSC–TiO<sub>2</sub> nanoparticle–implant complexes. The results showed TiO<sub>2</sub> nanoparticles significantly promoted the adhesion and proliferation of cell sheets, and upregulated the expression of osteogenic genes (alkaline phosphatase (ALP), osteocalcin (OCN), Collagen I, bone morphogenetic protein 2 (BMP2), runt-related transcription factor 2 (Runx2) and Osterix) ( $P < 0.05$ ). In *in vivo* studies, the results from micro-CT and hard tissue slices showed that the bone-implant contact (BIC) and bone volume per total volume (BV/TV) were significantly higher in the BMSC–TiO<sub>2</sub> nanoparticle–implant group compared with the BMSC–implant group ( $n = 6$ ,  $P < 0.05$ ). In conclusion, anatase TiO<sub>2</sub> nanoparticle surfaces could significantly improve the osseointegrating functionality of BMSC sheets. BMSC–TiO<sub>2</sub> nanoparticle–implant complexes are a potential and novel strategy for rapid osseointegration.

Received 7th May 2017  
Accepted 6th July 2017

DOI: 10.1039/c7ra05134d

rsc.li/rsc-advances

## 1. Introduction

Osseointegration is enhanced by a series of surface modifications, such as grit-blasting/thermo-chemical treatment,<sup>1</sup> grit-blasting/acid etching,<sup>2</sup> electrodeposits,<sup>3</sup> deposition by lasers,<sup>4</sup> and microarc oxidation.<sup>5</sup> Many studies have investigated the feasibility of applying cell sheets to bone regeneration,<sup>6</sup> cardiac regeneration,<sup>7</sup> cartilage regeneration,<sup>8</sup> tendon healing,<sup>9</sup> corneal regeneration,<sup>10</sup> esophageal regeneration,<sup>11</sup> periodontal regeneration,<sup>12</sup> and full thickness skin wound repair.<sup>13</sup> Recently, some studies<sup>14,15</sup> have reported bone marrow mesenchymal stem cell sheets (BMSC sheets) as a powerful tool for bioengineering applications in accelerating osseointegration.

In addition, previous studies confirmed that micro and nano structures on Ti substrates could enhance the biological responses of BMSCs.<sup>16–19</sup> It was reported that specific micro and nano structures with 80 nm grains significantly enhanced osteogenic differentiation of BMSCs compared

with 20 nm and 40 nm grains.<sup>20</sup> Nevertheless, to the best of our knowledge, no research has been conducted to investigate the effects of TiO<sub>2</sub> nanoparticle coated titanium implants on osseointegrating functionality of cell sheets *in vitro* and *in vivo*.

We choose BMSCs to investigate because BMSCs are multi-lineage differentiation potential cells that can be induced into osteoblasts, myoblasts, adipocytes, chondrocytes, tenocytes, and neurocytes.<sup>21–23</sup> Compared with terminally differentiated cells, BMSCs are immune-tolerated owing to the lack of MHC-II markers and low levels of MHC-I markers.<sup>24</sup> Moreover, BMSCs are quite easy to obtain, and culturing method is mature.<sup>25</sup> The process of osseointegration around implants includes hemostasis, inflammation, proliferation, and remodeling,<sup>26</sup> and BMSCs play a great role in the process of osseointegration. BMSCs migrate to the sites of titanium implants, and differentiate into osteoblasts. During osteogenic differentiation, BMSCs secrete the ECM, and express alkaline phosphatase and osteocalcin, which contribute to the acceleration of osseointegration.<sup>26</sup>

The aims of this study were to fabricate BMSC–TiO<sub>2</sub> nanoparticle–implant complexes by using light-induced cell sheet technology, and to investigate the effects of TiO<sub>2</sub> nanoparticle implants on osseointegrating functionality of BMSC sheets *in vitro* and *in vivo*.

<sup>a</sup>Department of Oral Medicine, Stomatology Hospital, School of Medicine, Zhejiang University, Yan'an Road, Hangzhou, P. R. China<sup>b</sup>Department of Implantology, Stomatology Hospital, School of Medicine, Zhejiang University, Yan'an Road, Hangzhou, P. R. China. E-mail: guo\_li1977@aliyun.com<sup>c</sup>Department of Oral and Maxillofacial Surgery, Stomatology Hospital, School of Medicine, Zhejiang University, Yan'an Road, Hangzhou, P. R. China

## 2. Materials and methods

### 2.1 Preparation of sandblasted, large-grit, and acid-etched (SLA) titanium disks/implants and TiO<sub>2</sub> nanoparticle coated titanium disks/implants

To obtain the SLA titanium disks and implants, disks were prepared from 1 mm thick and 2.5 cm diameter sheets of grade 2 unalloyed Ti, and implants were prepared from 2.2 mm diameter and 6 mm length grade 2 unalloyed Ti (Guangci, Ningbo, Zhejiang, China). The degreased disks and implants were grit-blasted with 0.25–0.50 mm corundum grits and subsequently conducted with double-acid etching. Briefly, titanium disks and implants were immersed in a 0.11 mol L<sup>-1</sup> ammonium fluoridic acid and 0.09 mol L<sup>-1</sup> nitric acid solution (Sigma-Aldrich, St. Louis, MO, USA) at room temperature, and then in a 5.8 mol L<sup>-1</sup> hydrochloric acid and 8.96 mol L<sup>-1</sup> sulfuric acid solution (Sigma-Aldrich, St. Louis, MO, USA) at 80 °C.

TiO<sub>2</sub> nanoparticle coated quartz substrates were prepared on the quartz substrates. TiO<sub>2</sub> nanoparticle coated titanium disks were prepared on SLA titanium disks. TiO<sub>2</sub> nanoparticle coated implants were prepared on SLA titanium implants. All surfaces were prepared through phase separation-induced self-assembly.<sup>27</sup> A precursor sol containing titanium tetrabutoxide (TBOT, Sinopharm Chemical Reagent, CP, >98%), acetylacetone (AcAc, Lingfeng Chemical Reagent, AR, >99%), and polyvinylpyrrolidone (PVP, K30, Sinopharm Chemical Reagent, AR, >99%) was spin-coated on the SLA titanium disks and implants at 8000 rpm for 40 s, and subsequently heated at 500 °C. Scanning electron microscopy (SEM) assay (SU-70, Hitachi, Japan) and energy-dispersive X-ray spectroscopy (EDS) assay were performed to characterize the SLA titanium disks/implants and TiO<sub>2</sub> nanoparticle coated titanium disks/implants. To collect the phase composition of the TiO<sub>2</sub> nanoparticle coated titanium disks, the X-ray diffractometer (XRD, PANalytical, X'Pert PRO) collected the XRD patterns of the samples. Raman spectra assay was conducted on the TiO<sub>2</sub> nanoparticle coated titanium disks by OMNIC software for dispersive Raman (Thermo Fisher Scientific, DXR532) with a 10 mW power at 532 nm.

### 2.2 Culture of BMSCs and fabrication of BMSC sheets

The Institutional Animal Care and Use Committee (Zhejiang University, Hangzhou, China) approved all animal experiments in this study according to "Experimental Animal Management Ordinance" issued by Chinese science and technology commission and "Laboratory Animal Science Guidance" issued by Chinese science and technology ministry. The method of isolation was reported elsewhere.<sup>25</sup> Briefly, three-week-old male Sprague-Dawley (SD) rats were anesthetized. BMSCs were aspirated from the bone marrow of tibias and femurs, and cultured in the basal medium (alpha-modified minimum essential medium (alpha-MEM; Gibco, USA) containing 10% fetal bovine serum (FBS; Gibco, USA), 1% penicillin (Gibco, USA), 1% streptomycin (Gibco, USA), and 0.272 g L<sup>-1</sup> L-glutamine (Sigma, USA)).

To fabricate BMSC sheets, 3 × 10<sup>4</sup> cells per cm<sup>2</sup> of BMSCs were seeded on the nanoparticle coated quartz substrates which were coated with 1.2 µg mL<sup>-1</sup> laminin-521 (Biolamina,

Sundbyberg, Sweden) in a 24-well plate. After culturing for 5 days, BMSC sheets were obtained through illumination under 5.5 mW cm<sup>-2</sup> power of UV365 nm for 30 min.<sup>28</sup> With light treatment, the surface of TiO<sub>2</sub> nanoparticles changed from electropositive to electronegative leading to the releasing of cell sheets.<sup>29</sup> The obtained cell sheets were used for subsequent experiments.

### 2.3 Adhesion and proliferation assay

Alamar Blue assay was conducted to evaluate the adhesion and proliferation of BMSC sheets cultured on SLA titanium disks and TiO<sub>2</sub> nanoparticle coated titanium disks. To evaluate the adhesive capacity, after culturing for 1 day, disks were picked up into a new 24-well plate. When we conducted proliferation assay, disks were not picked up. After culturing for 1, 3, and 7 days, the culture media was removed and samples were rinsed 3 times with 1 × PBS. Subsequently, 100 µL of Alamar Blue solution and 900 µL of fresh cell culture media were added to each well, and the mixture was incubated at 37 °C for 4 h. Then, the incubation solution was measured by a microplate reader at 540/590 nm. Medium supplemented with 10% Alamar Blue dye was used as a negative control.

### 2.4 Alkaline phosphatase (ALP) activity assay

To evaluate the effects of TiO<sub>2</sub> nanoparticles on osteogenic differentiation of BMSC sheets, we performed ALP activity assay. BMSC sheets were seeded in a 6-well plate on SLA titanium disks and TiO<sub>2</sub> nanoparticle coated titanium disks. After undergoing osteogenic differentiation for 7 and 14 days, BMSC sheets were lysed, and then total protein concentrations were determined using a bicinchoninic acid (BCA) kit (Pierce Biotechnology, Inc., USA). ALP activity was measured at 405 nm by *p*-nitrophenyl phosphate (Wako Pure Chemical Industries, Ltd., Japan) and normalized to the amount of total protein. The relative ALP activity was determined as follows: units per mg protein = concentration of *p*-nitrophenol released by sample (nmol µL<sup>-1</sup>)/(15 × protein concentration (µg µL<sup>-1</sup>)).

### 2.5 Quantitation of osteocalcin (OCN) using enzyme-linked immunosorbent assay (ELISA)

BMSC sheets were seeded in a 6-well plate on SLA titanium disks and TiO<sub>2</sub> nanoparticle coated titanium disks. After culturing in osteogenic medium for 14 and 21 days, the culture medium was collected and centrifuged at 3000 rpm, 4 °C for 10 min, and the concentrations of OCN were measured by ELISA kits (R&D Systems Inc., USA) according to the manufacturer's instructions. OCN concentrations were expressed as ng mL<sup>-1</sup> supernatant.

### 2.6 Reverse transcription and quantitative polymerase chain reaction (RT-qPCR)

Total RNA of BMSC sheets was extracted using TRIzol reagent (Invitrogen, USA). Half of one microgram of total RNA was reverse transcribed in a 10 µL reaction volume using the PrimeScript™ RT Reagent Kit (Perfect Real Time, TaKaRa, Dalian, China) according to the manufacturer's protocol. Real-



**Table 1** Nucleotide sequences for RT-qPCR primers

| Genes             | Sequences of primer (5'–3')   |
|-------------------|---|
| <i>ALP</i>        | Forward: TGGTACTCGGACAATGAGATGC<br>Reverse: GCTCTTCCAAATGCTGATGAGGT   |
| <i>Runx2</i>      | Forward: CAGTATGAGAGTAGGTGTCCCGC<br>Reverse: AAGAGGGGTAAGACTGGTCATAGG |
| <i>Collagen I</i> | Forward: CAGATTGAGAACATCCGCAGC<br>Reverse: CGGAACCTTCGCTTCCATACTC     |
| <i>BMP2</i>       | Forward: ACAAACGAGAAAAGCGTCAAGC<br>Reverse: CCCACATCACTGAAGTCCACATA   |
| <i>Osterix</i>    | Forward: CTGGGAAAAGGAGGCACAAAGA<br>Reverse: GGGGAAAGGGTGGGTAGTCATT    |
| <i>OCN</i>        | Forward: AGGGCAGTAAGGTGGTGAATAGA<br>Reverse: GAAGCCAATGTGGTCCGCTA     |
| <i>GAPDH</i>      | Forward: GGCACAGTCAAGGCTGAGAATG<br>Reverse: ATGGTGGTGAAGACGCCAGTA     |

time PCR was performed in the ABI ViiA™ 7 System (Applied Biosystems, Foster City, CA) by using a SYBR Green kit (TaKaRa, Tokyo, Japan). The primers are shown in Table 1. The relative gene expressions were analyzed using the  $2^{-\Delta\Delta C_T}$  method. After

normalization to GAPDH, the targeted genes were expressed as fold changes relative to controls.

## 2.7 Protein isolation and western blot analysis

Total proteins were extracted using RIPA buffer with phenylmethanesulfonyl fluoride (PMSF, Beyotime, China). Proteins were loaded and separated on Tris–glycine SDS-polyacrylamide gel (Invitrogen, USA), and subsequently transferred onto a polyvinylidene fluoride membrane (Millipore, USA) for immunoblotting. The primary antibodies (rat BMP2, Runx2, Collagen type I (Col-I) (Abcam, USA), and  $\beta$ -actin (Wuhan goodbio technology CO., LTD)) were used to incubate with membranes overnight at 4 °C. Then the peroxidase-conjugated secondary antibody (Wuhan goodbio technology CO., LTD) was used to incubate with the membranes for 1 h at room temperature. The blots were visualized using a chemiluminescent ECL reagent (Millipore, USA). Each target protein was normalized to  $\beta$ -actin.

## 2.8 Construction of BMSC–implant complexes

After BMSC sheets formed, the sheets detached from the substrates with the illumination of UV 365 nm. The detached

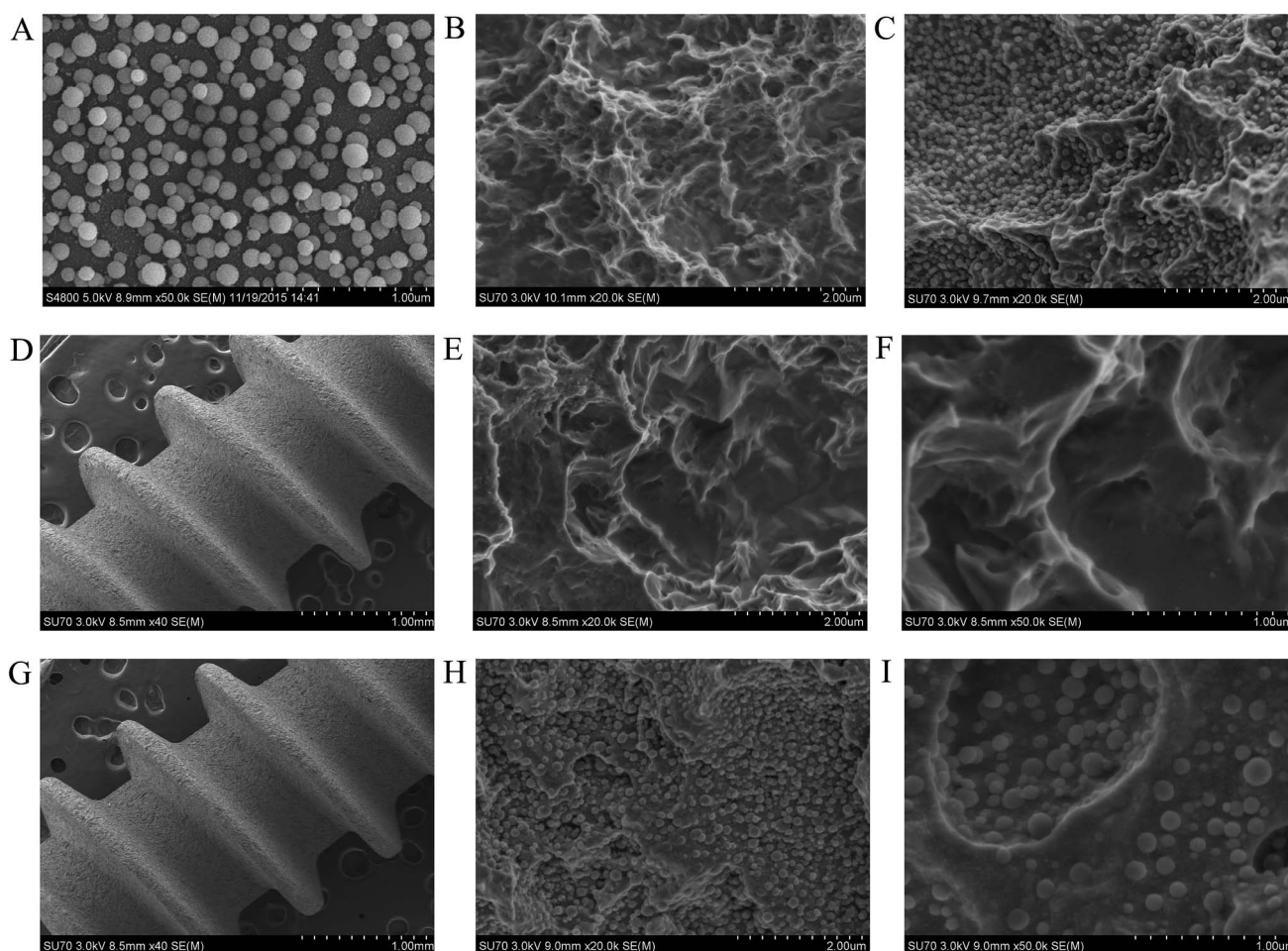


**Fig. 1** SEM images of different substrates. (A) TiO<sub>2</sub> nanoparticles on quartz substrates, (B) SLA titanium disks, (C) TiO<sub>2</sub> nanoparticle coated SLA titanium disks, (D–F) SLA titanium implants, (G–I) TiO<sub>2</sub> nanoparticle coated SLA titanium implants. Scale bar: (A, F and I) 1 μm; (B, C, E and H) 2 μm; (D and G) 1 mm.





BMSC sheets floated in 1 mL  $1\times$  PBS in a 24-well plate. We took the substrate away and put a SLA or  $\text{TiO}_2$  nanoparticle-coated implant under the floating BMSC sheet. Then the implant was picked up gradually with sterilized tweezers, and BMSC sheets attached with the implant. The obtained BMSC-implant complexes were cultured in an incubator for half of an hour with 50  $\mu\text{L}$  basal medium in a 6 cm culture dish. After the cell sheet attached well with the implant, the BMSC-implant complexes were then cultured in basal medium for 7 days.

## 2.9 Transplantation of BMSC-implant complexes

A total of 24 male SD rats were used for *in vivo* evaluation. 10% sterile chloral hydrate solution was intra-abdominally injected into the rats at a dose of 3.5 mL  $\text{kg}^{-1}$ . The implant cavity was prepared by 2.2 mm diameter drills. Two kinds of implants (BMSC-implant complexes, and BMSC- $\text{TiO}_2$  nanoparticle-implant complexes,  $n = 6$  per group) were inserted into tibias about 7 mm below the knee joints. Each rat received 1 implant in each tibia.

## 2.10 Micro-CT scan and hard tissue slices

To prepare specimens, the rat tibias were removed and fixed in a 4% paraformaldehyde solution for 48 h at room temperature. The microtomographical reconstruction was performed with micro-CT (Scanco Medical, Switzerland,  $\mu\text{CT}$ -100). The parameter settings were 70 kV, 200  $\mu\text{A}$  at a resolution of 14.8  $\mu\text{m}$  and exposure time of 300 ms. The newly formed bone was restricted to a circle with radius of 0.5 mm surrounding the implants. At a 3-dimensional (3D) level, osseointegration was determined using bone-implant contact (BIC) and bone volume per total volume (BV/TV) by Evaluation v6.5-3 (Scanco Medical, Switzerland).

Following the micro-CT testing, specimens were dehydrated with ethanol solutions and embedded with methyl methacrylate (MMA) to solidify. The specimens were placed in a horizontal position and cut into 4  $\mu\text{m}$  thick sections using Leica SP1600 (Leica, Germany) and processed with toluidine blue and Masson's trichrome staining. The image analysis software Image-Pro Plus (version 6.0; Media Cybernetics; Rockville, MD; USA) was used to evaluate the BIC and BV/TV of implants.

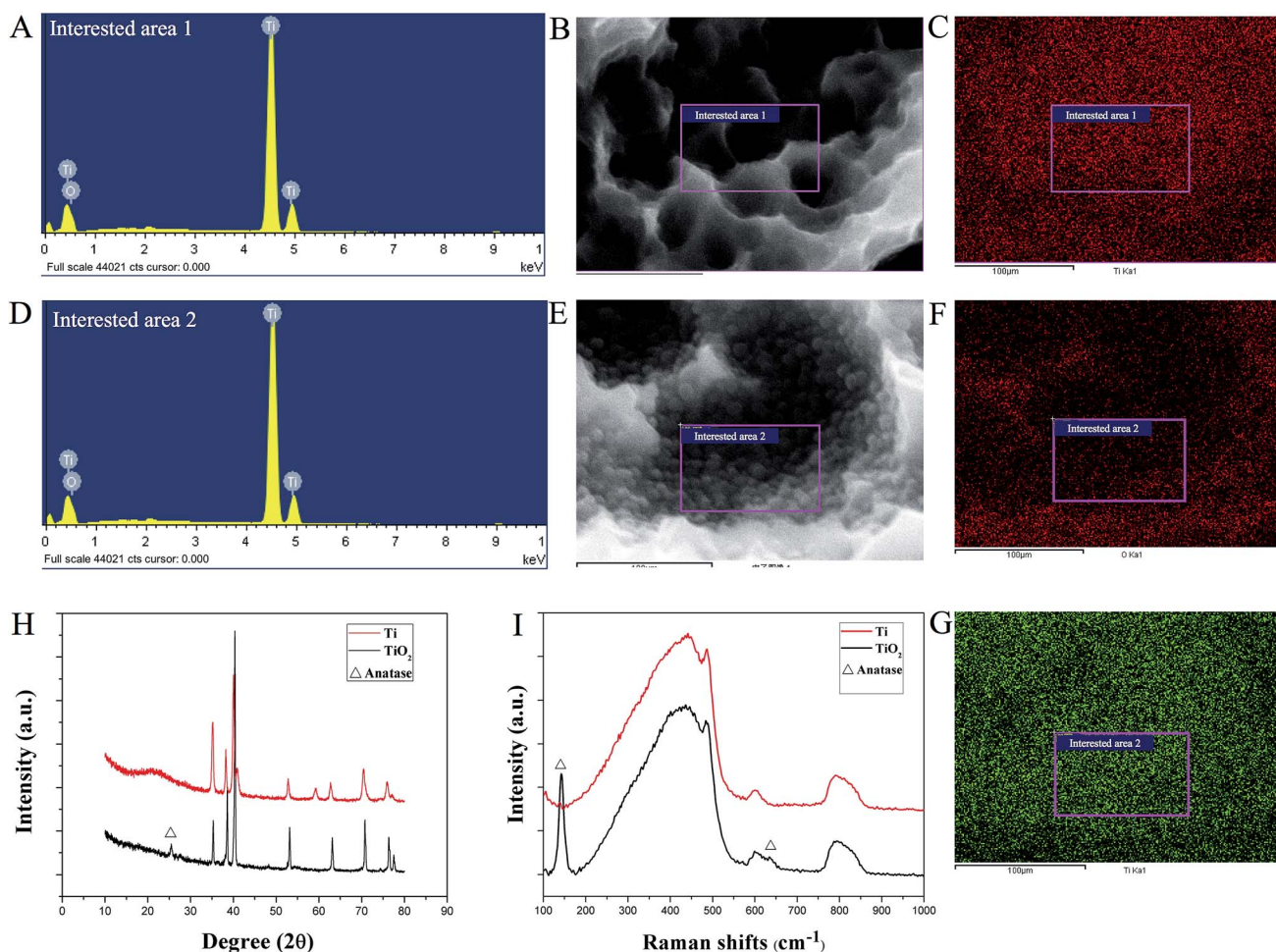


**Fig. 2** Characteristics of SLA titanium disks and  $\text{TiO}_2$  nanoparticle coated SLA titanium disks. (A–F) EDS analysis of SLA titanium disks, and  $\text{TiO}_2$  nanoparticle coated SLA titanium disks. (C) Mapping of Ti element on SLA titanium disks. (F) Mapping of oxygen element on  $\text{TiO}_2$  nanoparticle coated SLA titanium disks. (G) Mapping of Ti element on  $\text{TiO}_2$  nanoparticle coated SLA titanium disks. (H) XRD patterns and (I) Raman spectra of SLA titanium disks and  $\text{TiO}_2$  nanoparticle coated SLA titanium disks.  $\Delta$ : peaks of anatase. Scale bar: (B, C and E–G) 100  $\mu\text{m}$ .



### 2.11 Statistical analysis

Data were obtained from at least 3 independent experiments and expressed as mean  $\pm$  standard deviation. Analysis was conducted using the SPSS 17.0 software package by one-way ANOVA with Bonferroni's post-hoc test (multiple comparisons) and unpaired Student's *t*-test (comparison between two groups). Differences were considered statistically significant at  $P < 0.05$ .

## 3. Results

### 3.1 Morphology of TiO<sub>2</sub> nanoparticle coated films, SLA titanium disks, TiO<sub>2</sub> nanoparticle coated titanium disks, SLA titanium implants, and TiO<sub>2</sub> nanoparticle coated implants

Fig. 1 illustrated the morphology of SLA surfaces and TiO<sub>2</sub> nanoparticle surfaces. The films showed homogeneous distribution of the TiO<sub>2</sub> nanoparticles. The diameter of nanoparticles was approximately 80–150 nm. After sandblasting and acid-etching treatment, the surface became rough and irregular, and small holes with micro pits (1–2  $\mu$ m in diameter) were observed under high magnification. In the holes and micro pits, the TiO<sub>2</sub> nanoparticles were clearly observed.

### 3.2 EDS analysis and crystalline phases of SLA titanium disks and TiO<sub>2</sub> nanoparticle coated titanium disks

Traces of oxygen were detected on the SLA surface under EDS analysis (Fig. 2A–G). The mapping of oxygen was consistent with the distribution of TiO<sub>2</sub> nanoparticles on the SLA titanium

disks. At 500 °C, the peaks at  $2\theta = 25.35^\circ$  corresponded to the (101) plane of anatase (Fig. 2H). The anatase phase of TiO<sub>2</sub> was also identified through Raman spectra. As shown in Fig. 2I, TiO<sub>2</sub> nanoparticle disks showed strong Raman shifts at 144  $\text{cm}^{-1}$ , which were ascribed to the  $E_g$  mode of the anatase phase (the shift at 144  $\text{cm}^{-1}$  was the strongest for the anatase phase). However, the typical peak of rutile located at 143  $\text{cm}^{-1}$  overlapped with the 144  $\text{cm}^{-1}$  peak of anatase. Another weak Raman shift was at 637  $\text{cm}^{-1}$ . Such Raman results were in good consistence with the XRD patterns.

### 3.3 Effects of TiO<sub>2</sub> nanoparticles on adhesion, proliferation, and osteogenic differentiation of BMSC sheets

The results of adhesion assay showed that TiO<sub>2</sub> nanoparticles significantly increased the adhesive capacity of BMSC sheets (Fig. 3A;  $P < 0.05$ ). The proliferation of BMSC sheets on TiO<sub>2</sub> nanoparticle coated titanium disks was elevated on days 5 and 7 (Fig. 3B;  $P < 0.05$ ). The ALP expression was also significantly increased on days 3 and 7 in the TiO<sub>2</sub> nanoparticle group compared with the SLA group (Fig. 3C;  $P < 0.05$ ), while the expression of OCN protein increased on days 14 and 21 (Fig. 3D;  $P < 0.05$ ). Fig. 6A–C showed that the mRNA levels of *ALP*, *BMP2*, *Collagen I*, *Runx2*, and *Osterix* significantly increased on days 3, 7, and 14 in the TiO<sub>2</sub> nanoparticle group, while the mRNA levels of *OCN* significantly increased on day 14 ( $P < 0.05$ ). Furthermore, the western blot results revealed that the proteins (Collagen I, BMP2, Runx2, and Osterix) were significantly up-regulated in the TiO<sub>2</sub> nanoparticle group on days 3, 7, and 14 (Fig. 4D). The

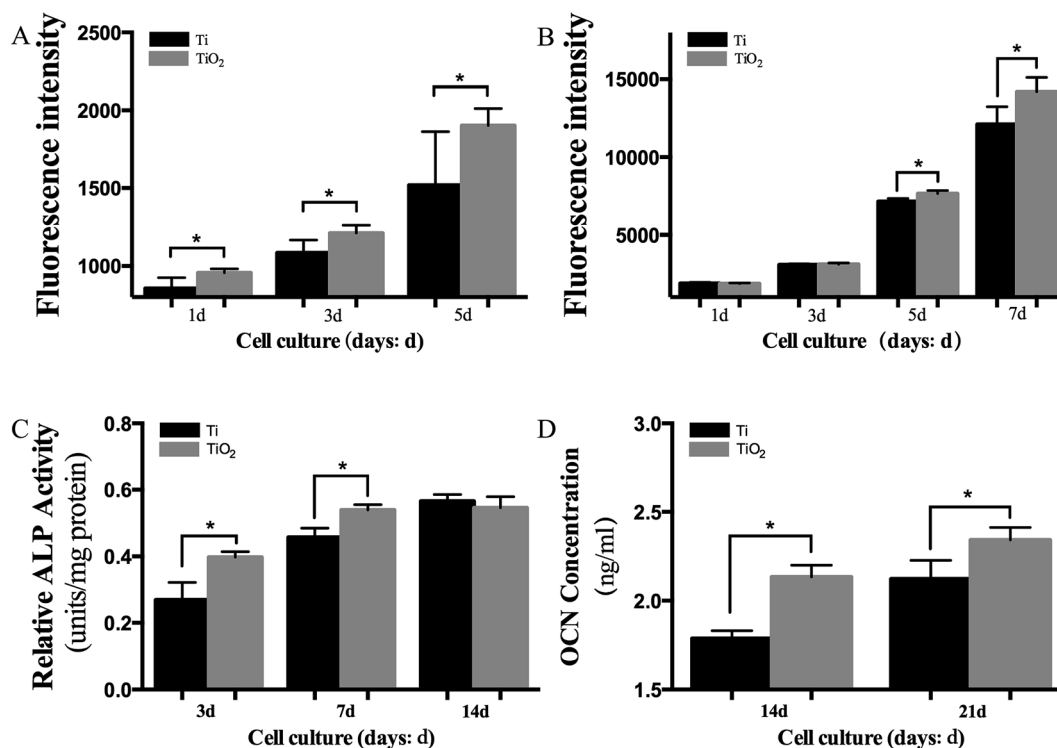


Fig. 3 (A) Adhesion assay on TiO<sub>2</sub> nanoparticle coated titanium disks at days 1, 3, and 5. (B) Proliferation of BMSC sheets on TiO<sub>2</sub> nanoparticle coated titanium disks measured by Alamar Blue at days 1, 3, 5, and 7. Effects of TiO<sub>2</sub> nanoparticle coated titanium disks on (C) relative ALP activity at days 3, 7, and 14, and (D) OCN concentration at days 14, and 21. \* $P < 0.05$ .



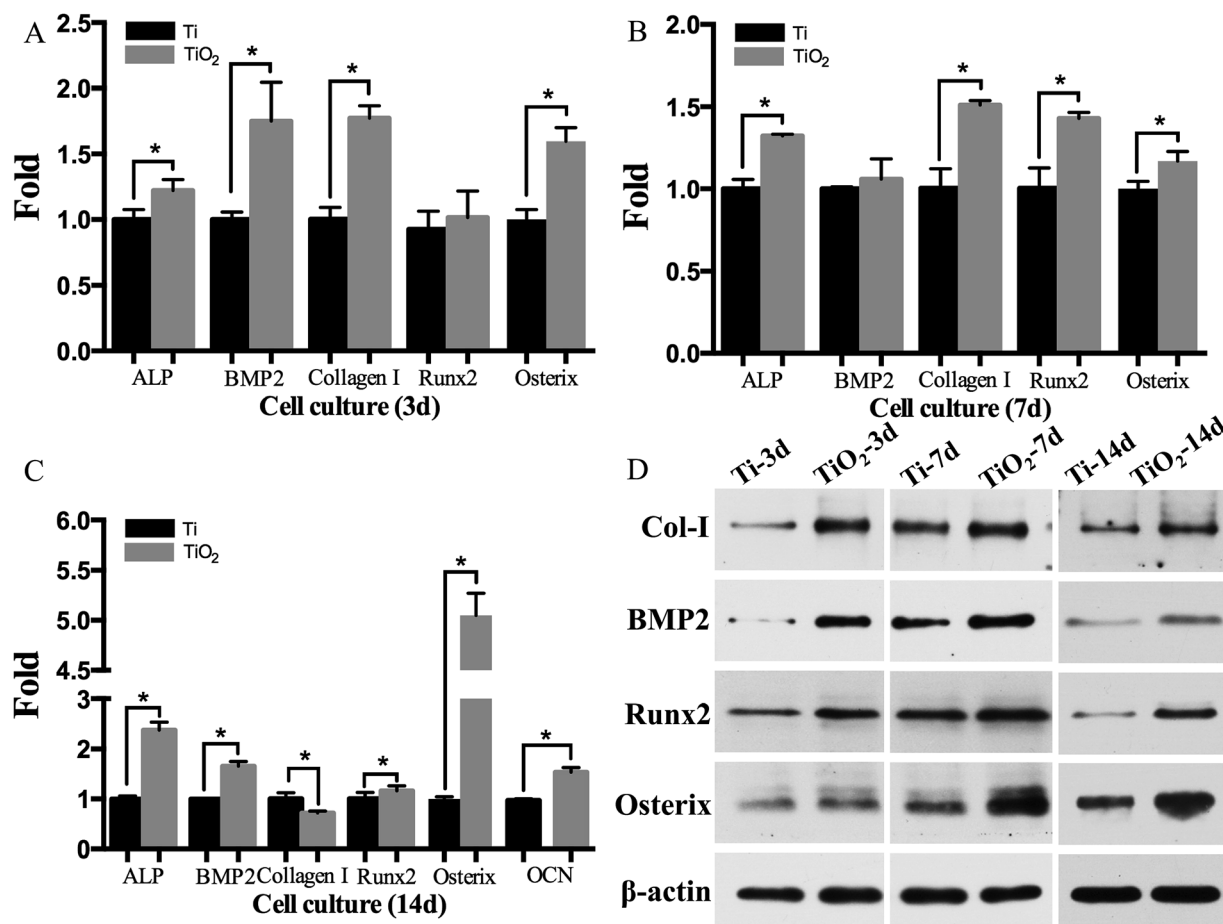


Fig. 4 Relative mRNA expression levels of ALP, BMP2, Collagen I, Runx2, Osterix, and OCN on SLA titanium disks and TiO<sub>2</sub> nanoparticle coated SLA titanium disks at (A) day 3, (B) day 7, and (C) day 14 compared with the SLA titanium disk group. (D) Western blot analysis of Col-I, BMP2, Runx2, and Osterix after 3, 7, and 14 days of osteogenic induction. \* $P < 0.05$ .

stimulating effects of TiO<sub>2</sub> on osteogenic genes indicated that TiO<sub>2</sub> nanoparticle coated titanium disks could significantly promote osteogenic differentiation of BMSC sheets *in vitro*.

### 3.4 Performance of BMSC-TiO<sub>2</sub> nanoparticle-implant complexes

The osseointegration was evaluated by the micro-CT and hard tissue slices after 1 month and 2 months of healing (Fig. 5 and 6). In the BMSC-TiO<sub>2</sub> nanoparticle-implant group, more bones contacted with implants than in the BMSC-implant group after 1 month of healing (Fig. 5A, B and 6A). Moreover, more surrounding bones in the BMSC-TiO<sub>2</sub> nanoparticle-implant group were discovered compared with the BMSC-implant group after 2 months of healing (Fig. 5C, D and 6B). In the Fig. 5E, F and 6C, D, the BIC and BV/TV values of the BMSC-TiO<sub>2</sub> nanoparticle-implant group were higher than BMSC-implant group ( $P < 0.05$ ).

## 4. Discussion

In this study, we developed a novel, simple, and effective method to fabricate rat BMSC-TiO<sub>2</sub> nanoparticle-implant

complexes. According to our data, anatase TiO<sub>2</sub> nanoparticle coated surfaces showed enhanced osseointegrating ability, and BMSC-TiO<sub>2</sub> nanoparticle-implant complexes provided an alternative novel strategy for potential rapid osseointegration.

In this study, we proved anatase TiO<sub>2</sub> nanoparticle coated surfaces effective for promoting osteogenic differentiation of BMSC sheets. There are several reasons for this. Firstly, anatase TiO<sub>2</sub> contributed to better osteogenic abilities when compared with the rutile TiO<sub>2</sub>.<sup>30</sup> Secondly, the hierarchical micro/nano-topographies contributed to enhancing osteogenesis. Some studies have documented the effects of micro/nano-topographies on osteogenesis *in vitro*.<sup>16–18</sup> The micro and nanoscale surfaces matched the natural structure of bone, which consisted of hierarchical structures such as nano-structures (including collagen, non-collagenous organic proteins, and mineral crystals) and micro-structures (including haversian systems, osteons, and single trabeculae). Thirdly, micro/nano hierarchical surfaces have great potential for improving spreading and osteogenic differentiation of BMSC sheets. Fourthly, UV-activated TiO<sub>2</sub> itself has excellent antibacterial activity. UV-activated TiO<sub>2</sub> has been used for killing a wide range of Gram-negative and Gram-positive bacteria, filamentous and unicellular fungi, algae, protozoa,





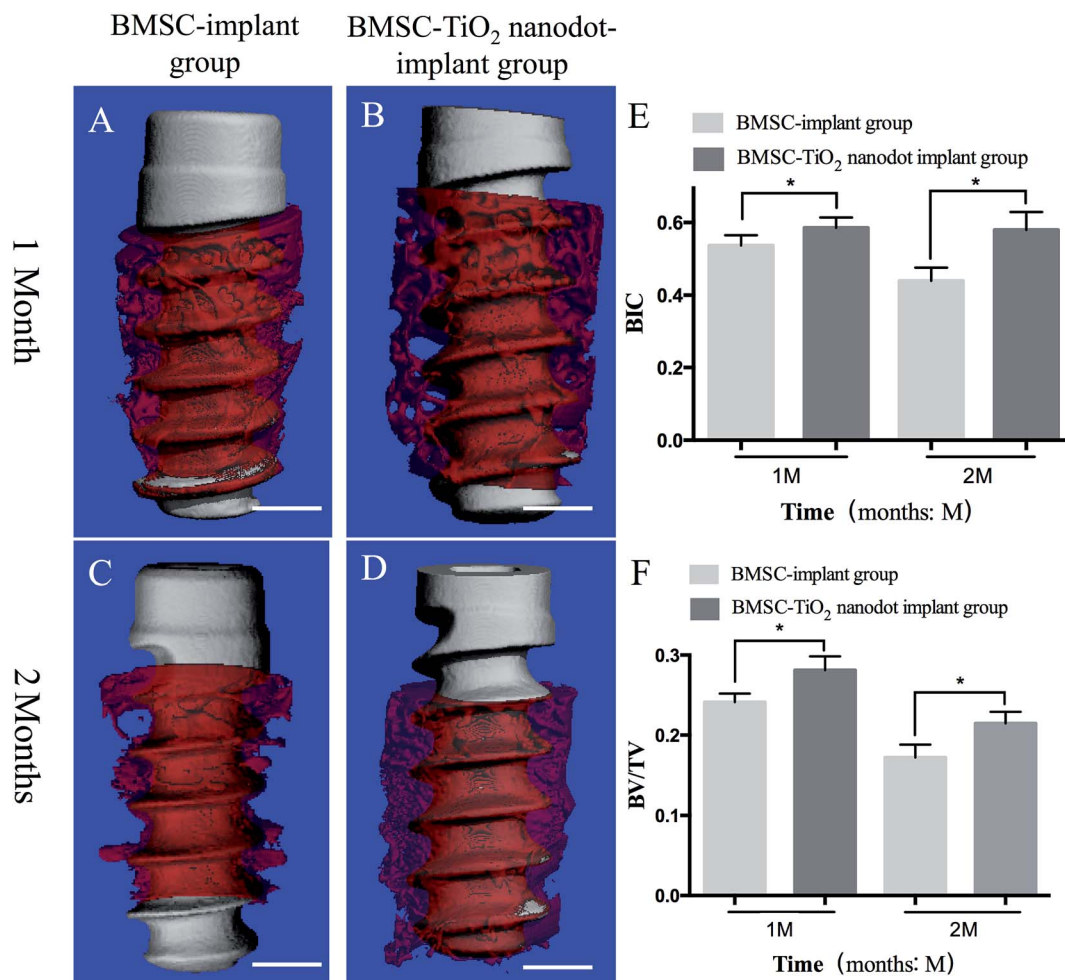


Fig. 5 BMSC-implant complexes and BMSC-TiO<sub>2</sub> nanoparticle-implant complexes were measured by micro-CT. The amount of bones surrounding inserted implants was larger in (B and D) the BMSC-TiO<sub>2</sub> nanoparticle-implant group than in (A and C) the control group. According to the analysis of micro-CT, BV/TV and BIC of the BMSC-TiO<sub>2</sub> nanoparticle-implant group were obviously higher than the BMSC-implant group after 1 month and 2 months of healing. (E) BIC and (F) BV/TV values of the two implant groups. Scale bar: (A–D) 1 mm, \**P* < 0.05.

mammalian viruses, and bacteriophage.<sup>31,32</sup> However, the toxic kinetics of TiO<sub>2</sub> nanoparticles has not yet been investigated. Therefore, since we do not know whether it is safe when used *in vivo*, the safety of TiO<sub>2</sub> nanoparticle coated implants will be measured in our future study.

BMSC sheets have been proven beneficial for cell-based tissue engineering, owing to the ability of multi-lineage potential<sup>33</sup> and preserving abundant ECM.<sup>34,35</sup> Meanwhile, BMSCs secrete quantities of growth factors effective at promoting osteogenic differentiation, bone matrix synthesis, and mineralization, such as BMP2, ALP, and OCN.<sup>36,37</sup> In our study, BMSC-TiO<sub>2</sub> nanoparticle-implant groups have elevated expression of BMP2, ALP, and OCN, thus providing a beneficial condition for osseointegration. Moreover, Zhou<sup>38</sup> reported that BMSCs could inhibit inflammation through BMSC-derived 15d-PGJ2 activation of the PPAR-γ receptor. Furthermore, Goodwin<sup>39</sup> reported that BMSCs could reduce inflammation by influencing antigen-specific CD4 T lymphocyte differentiation. Overall, these factors potentially promote a beneficial biological environment for osseointegration.

We chose the male rat model in this study. We found an interesting phenomenon that tibias became longer when rats grew older. At the same time, distance from the metaphysis to implants became larger. The decreasing BIC and BV/TV could be explained by this phenomenon. Clotkie<sup>40</sup> compared various bones from SD rats of different weights (*i.e.*, 100 g, 200 g, 300 g, 350 g), and found that the tibial plateau of 350 g rats was a good recipient site. However, the study only evaluated osseointegration at 6 weeks. Yu<sup>14</sup> used Wistar rats (200–250 g) to evaluate osseointegration at 4 and 8 weeks. They did not find similar phenomenon. This discrepancy may be due to using different strains of rats.

Furthermore, the molecular mechanisms of the effects of anatase TiO<sub>2</sub> nanoparticles on osseointegration were not investigated in this study. In order to fully link the surface modifications to observations, we will evaluate the effects of specific genes on osseointegration through inhibition and overexpression in the future study.

In this study, we successfully constructed BMSC-TiO<sub>2</sub> nanoparticle-implant complexes using light-induced cell sheet



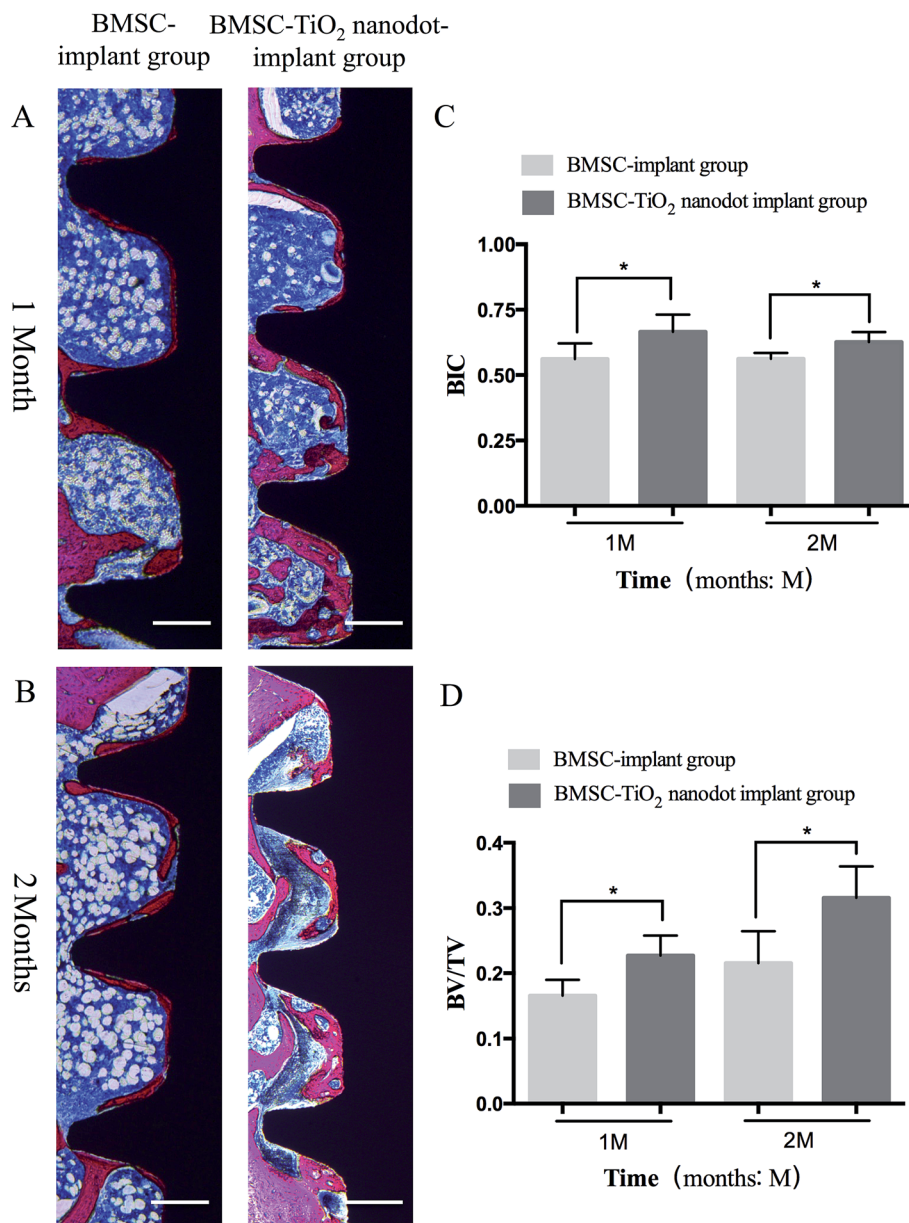


**Fig. 6** Hard tissue slices were used to evaluate the osseointegration of BMSC-implants and BMSC-TiO<sub>2</sub> nanoparticle-implants ((A) 1 month; (B) 2 months). More contacting bones were observed in the BMSC-TiO<sub>2</sub> nanoparticle-implant group than BMSC-implant group after (A) 1 month and (B) 2 months of healing. According to the analysis of hard tissue slices, the (C) BIC and (D) BV/TV of the BMSC-TiO<sub>2</sub> nanoparticle-implant group were higher than the BMSC-implant group. Scale bar: 300  $\mu$ m. \* $P$  < 0.05.

technology. Our BMSC-TiO<sub>2</sub> nanoparticle-implant complexes were a potential and novel strategy for accelerating osseointegration.

## 5. Conclusions

Within the limits of the present investigation we concluded that anatase TiO<sub>2</sub> nanoparticle coated titanium surfaces significantly enhanced osteogenic differentiation of BMSC sheets *in vitro* and enhanced bone formation *in vivo*. These findings indicated that BMSC-TiO<sub>2</sub> nanoparticle-implant complexes

possessed potential for improving biocompatibility of titanium implants.

## Conflict of interest

There are no conflicts of interest to declare.

## Acknowledgements

This work was supported by the National Natural Science Foundation of China (Grant No. 81272157 and 31470945) and the Health Department of Zhejiang Province Fund (Grant





No. 2015KYA147 and 2014KYA127). We thank LetPub (www.letpub.com) for its linguistic assistance during the preparation of this manuscript.

## References

- 1 F. J. Gil, D. D. S. P. Eduardo Espinar, D. D. S. P. Jose Maria Llamas and P. Sevilla, *Clinical Implant Dentistry and Related Research*, 2014, **16**, 273–281.
- 2 D. Yoo, C. Marin, G. Freitas, N. Tovar, E. A. Bonfante, H. S. Teixeira, M. N. Janal and P. G. Coelho, *Implant Dent.*, 2015, **24**, 256–262.
- 3 Z. Shifang, S. Jue, H. Fuming, L. Liu and Y. Guoli, *J. Biomed. Nanotechnol.*, 2014, **10**, 1313–1319.
- 4 F. Sima, P. M. Davidson, J. Dentzer, R. Gadiou, E. Pauthe, O. Gallet, I. N. Mihailescu and K. Anselme, *ACS Appl. Mater. Interfaces*, 2015, **7**, 911–920.
- 5 R. Zhou, D. Wei, S. Cheng, W. Feng, Q. Du, H. Yang, B. Li, Y. Wang, D. Jia and Y. Zhou, *ACS Appl. Mater. Interfaces*, 2014, **6**, 4797–4811.
- 6 Q. Xie, Z. Wang, Y. Huang, X. Bi, H. Zhou, M. Lin, Z. Yu, Y. Wang, N. Ni, J. Sun, S. Wu, Z. You, C. Guo, H. Sun, Y. Wang, P. Gu and X. Fan, *Biomaterials*, 2015, **66**, 67–82.
- 7 K. Matsuura, F. Kodama, K. Sugiyama, T. Shimizu, N. Hagiwara and T. Okano, *Tissue Eng., Part C*, 2015, **21**, 330–338.
- 8 F. Yano, H. Hojo, S. Ohba, T. Saito, M. Honnami, M. Mochizuki, T. Takato, H. Kawaguchi and U. I. Chung, *Biomaterials*, 2013, **34**, 5581–5587.
- 9 I. Komatsu, J. H. Wang, K. Iwasaki, T. Shimizu and T. Okano, *Acta Biomater.*, 2016, **42**, 136–146.
- 10 T. Kobayashi, K. Kan, K. Nishida, M. Yamato and T. Okano, *Biomaterials*, 2013, **34**, 9010–9017.
- 11 N. Kanai, M. Yamato and T. Okano, *Ann. Transl. Med.*, 2014, **2**, 28.
- 12 H. Zhang, S. Liu, B. Zhu, Q. Xu, Y. Ding and Y. Jin, *Stem Cell Res. Ther.*, 2016, **7**, 168.
- 13 L. Chen, Q. Xing, Q. Zhai, M. Tahtinen, F. Zhou, L. Chen, Y. Xu, S. Qi and F. Zhao, *Theranostics*, 2017, **7**, 117–131.
- 14 M. Yu, W. Zhou, Y. Song, F. Yu, D. Li, S. Na, G. Zou, M. Zhai and C. Xie, *Bone*, 2011, **49**, 387–394.
- 15 W. Zhou, C. Han, Y. Song, X. Yan, D. Li, Z. Chai, Z. Feng, Y. Dong, L. Li, X. Xie, F. Chen and Y. Zhao, *Biomaterials*, 2010, **31**, 3212–3221.
- 16 N. Ren, S. Zhang, Y. Li, S. Shen, Q. Niu, Y. Zhao and L. Kong, *Br. J. Oral and Maxillofac. Surg.*, 2014, **52**, 907–912.
- 17 L. Zhao, S. Mei, P. K. Chu, Y. Zhang and Z. Wu, *Biomaterials*, 2010, **31**, 5072–5082.
- 18 L. Zhao, L. Liu, Z. Wu, Y. Zhang and P. K. Chu, *Biomaterials*, 2012, **33**, 2629–2641.
- 19 G. Li, H. Cao, W. Zhang, X. Ding, G. Yang, Y. Qiao, X. Liu and X. Jiang, *ACS Appl. Mater. Interfaces*, 2016, **8**, 3840–3852.
- 20 X. Shen, P. Ma, Y. Hu, G. Xu, J. Zhou and K. Cai, *Colloids Surf., B*, 2015, **127**, 221–232.
- 21 G. Kaur, M. T. Valarmathi, J. D. Potts, E. Jabbari, T. Sabo-Attwood and Q. Wang, *Biomaterials*, 2010, **31**, 1732–1741.
- 22 P. Sreejit, K. B. Dilip and R. S. Verma, *Cell Tissue Res.*, 2012, **350**, 55–68.
- 23 Y. Jiang, B. N. Jahagirdar, R. L. Reinhardt, R. E. Schwartz, C. D. Keene, X. R. Ortiz-Gonzalez, M. Reyes, T. Lenvik, T. Lund, M. Blackstad, J. Du, S. Aldrich, A. Lisberg, W. C. Low, D. A. Largaespada and C. M. Verfaillie, *Nature*, 2002, **418**, 41–49.
- 24 K. Thejaswi, M. Amarnath, G. Srinivas, M. K. Jerald, T. A. Raj and S. Singh, *Cell Tissue Transplant. Ther.*, 2012, **4**, 1–13.
- 25 D. P. Lennon and A. I. Caplan, *Exp. Hematol.*, 2006, **34**, 1606–1607.
- 26 R. Tejero, E. Anitua and G. Orive, *Prog. Polym. Sci.*, 2014, **39**, 1406–1447.
- 27 K. Zhu, N. R. Neale, A. Miedaner and A. J. Frank, *Nano Lett.*, 2007, **7**, 69–74.
- 28 Z. Jiang, Y. Xi, K. Lai, Y. Wang, H. Wang and G. Yang, *BioMed Res. Int.*, 2017, **2017**, 9474573.
- 29 Y. Hong, M. F. Yu, W. J. Weng, K. Cheng, H. M. Wang and J. Lin, *Biomaterials*, 2013, **34**, 11–18.
- 30 L. Lv, K. Li, Y. Xie, Y. Cao and X. Zheng, *Mater. Sci. Eng., C*, 2017, **78**, 96–104.
- 31 H. A. Foster, I. B. Ditta, S. Varghese and A. Steele, *Appl. Microbiol. Biotechnol.*, 2011, **90**, 1847–1868.
- 32 J. C. Yu, W. Ho, J. Lin, H. Yip and P. K. Wong, *Environ. Sci. Technol.*, 2003, **37**, 2296–2301.
- 33 F. Wei, C. Qu, T. Song, G. Ding, Z. Fan, D. Liu, Y. Liu, C. Zhang, S. Shi and S. Wang, *J. Cell. Physiol.*, 2012, **227**, 3216–3224.
- 34 J. Chen, D. Zhang, Q. Li, D. Yang, Z. Fan, D. Ma and L. Ren, *Tissue Cell*, 2016, **48**, 442–451.
- 35 J. Ren, P. Jin, M. Sabatino, A. Balakumaran, J. Feng, S. A. Kuznetsov, H. G. Klein, P. G. Robey and D. F. Stronck, *Cytotherapy*, 2011, **13**, 661–674.
- 36 Y. Liu, L. Ming, H. Luo, W. Liu, Y. Zhang, H. Liu and Y. Jin, *Biomaterials*, 2013, **34**, 9998–10006.
- 37 J. Yan, C. Zhang, Y. Zhao, C. Cao, K. Wu, L. Zhao and Y. Zhang, *Biomaterials*, 2014, **35**, 7734–7749.
- 38 J. Zhou, L. Jiang, X. Long, C. Fu, X. Wang, X. Wu, Z. Liu, F. Zhu, J. Shi and S. Li, *J. Cell. Mol. Med.*, 2016, **20**, 1706–1717.
- 39 M. Goodwin, V. Sueblinvong, P. Eisenhauer, N. P. Ziats, L. Leclair, M. E. Poynter, C. Steele, M. Rincon and D. J. Weiss, *Stem Cells*, 2011, **29**, 1137–1148.
- 40 C. M. Clokie and H. Warshawsky, *Compendium-continuing Education for Veterinarians*, 1995, vol. 16.

